Science Advances

AAAS

advances.sciencemag.org/cgi/content/full/4/5/eaap9264/DC1

Supplementary Materials for

Ultrahigh-performance transparent conductive films of carbon-welded isolated single-wall carbon nanotubes

Song Jiang, Peng-Xiang Hou, Mao-Lin Chen, Bing-Wei Wang, Dong-Ming Sun, Dai-Ming Tang, Qun Jin, Qing-Xun Guo, Ding-Dong Zhang, Jin-Hong Du, Kai-Ping Tai, Jun Tan, Esko I. Kauppinen, Chang Liu, Hui-Ming Cheng

Published 4 May 2018, *Sci. Adv.* **4**, eaap9264 (2018)
DOI: 10.1126/sciadv.aap9264

The PDF file includes:

Other Supplementary Material for this manuscript includes the following:
(available at advances.sciencemag.org/cgi/content/full/4/5/eaap9264/DC1)

- movie S1 (.mp4 format). Bending test of SWCNT OLED.

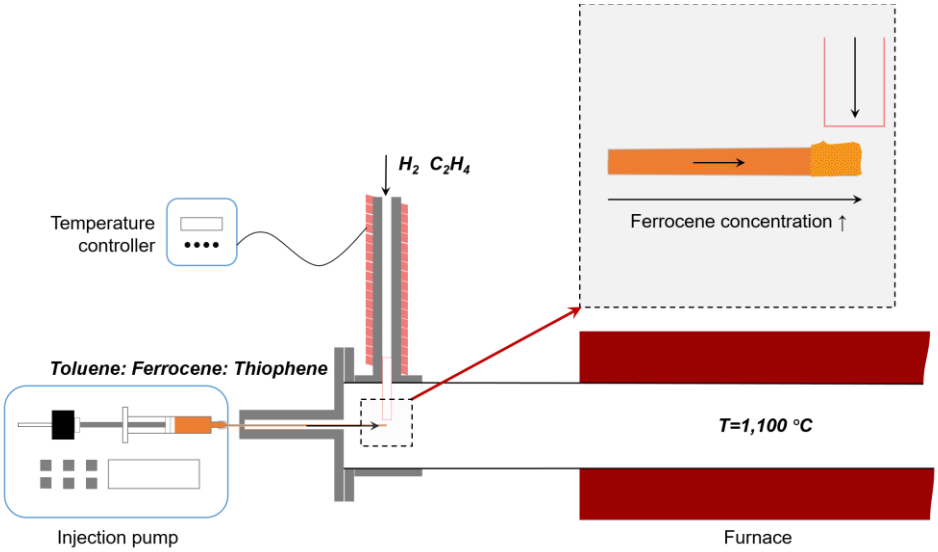

fig. S1. Experimental setup for SWCNT synthesis. The injection-FCCVD method with heated high-flux gases ensures the synthesis of high-quality SWCNT films.

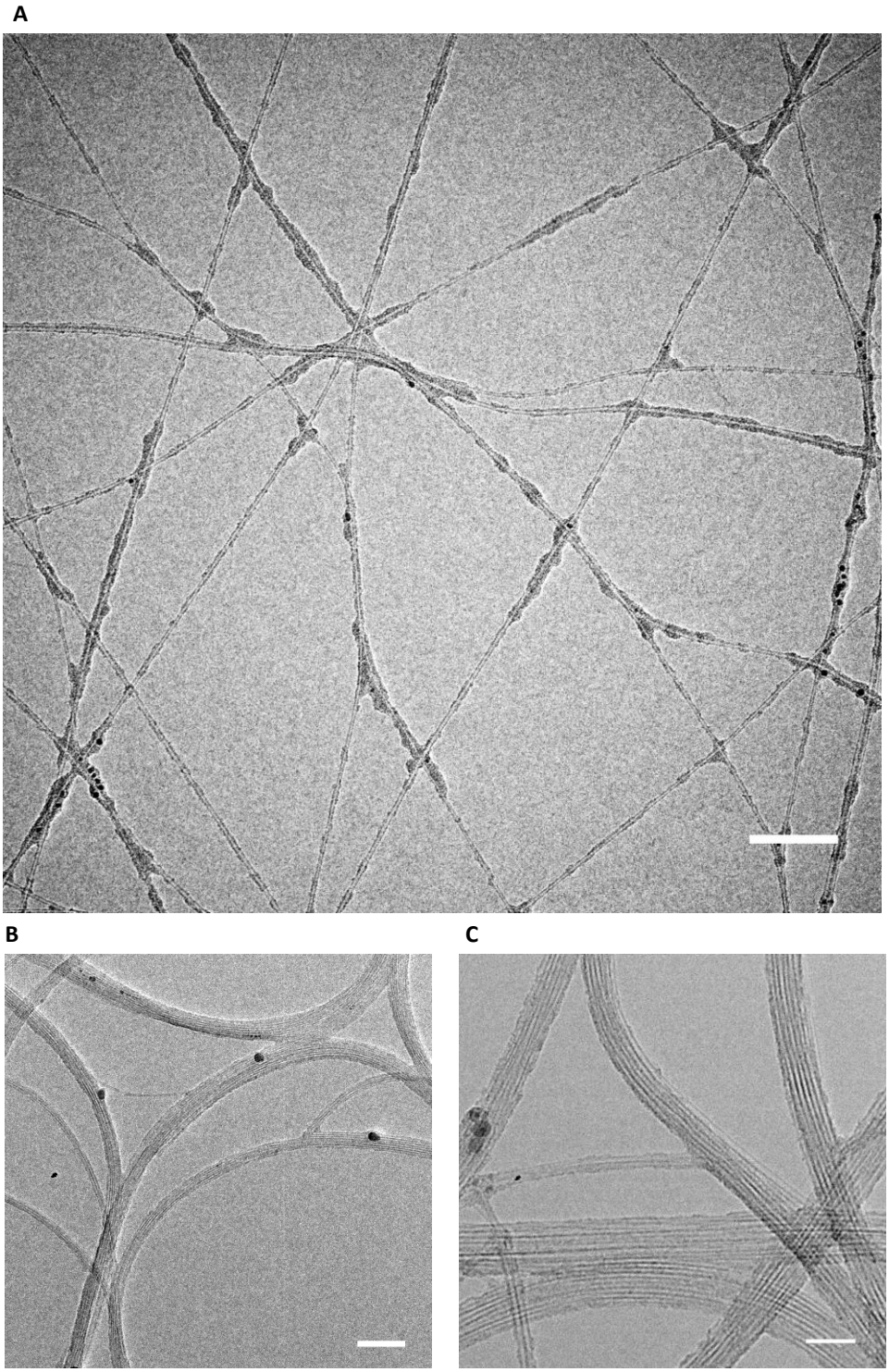

fig. S2. Typical TEM images of different SWCNTs. (**A**) Typical TEM image of isolated SWCNTs with carbon-welded joints. The scale bar is 50 nm. (**B** and **C**) Typical TEM images of normal bundled SWCNTs. The respective scale bars in (B) and (C) are 50 nm and 20 nm. Entangled SWCNT bundles with diameters of ~20 nm are observed.

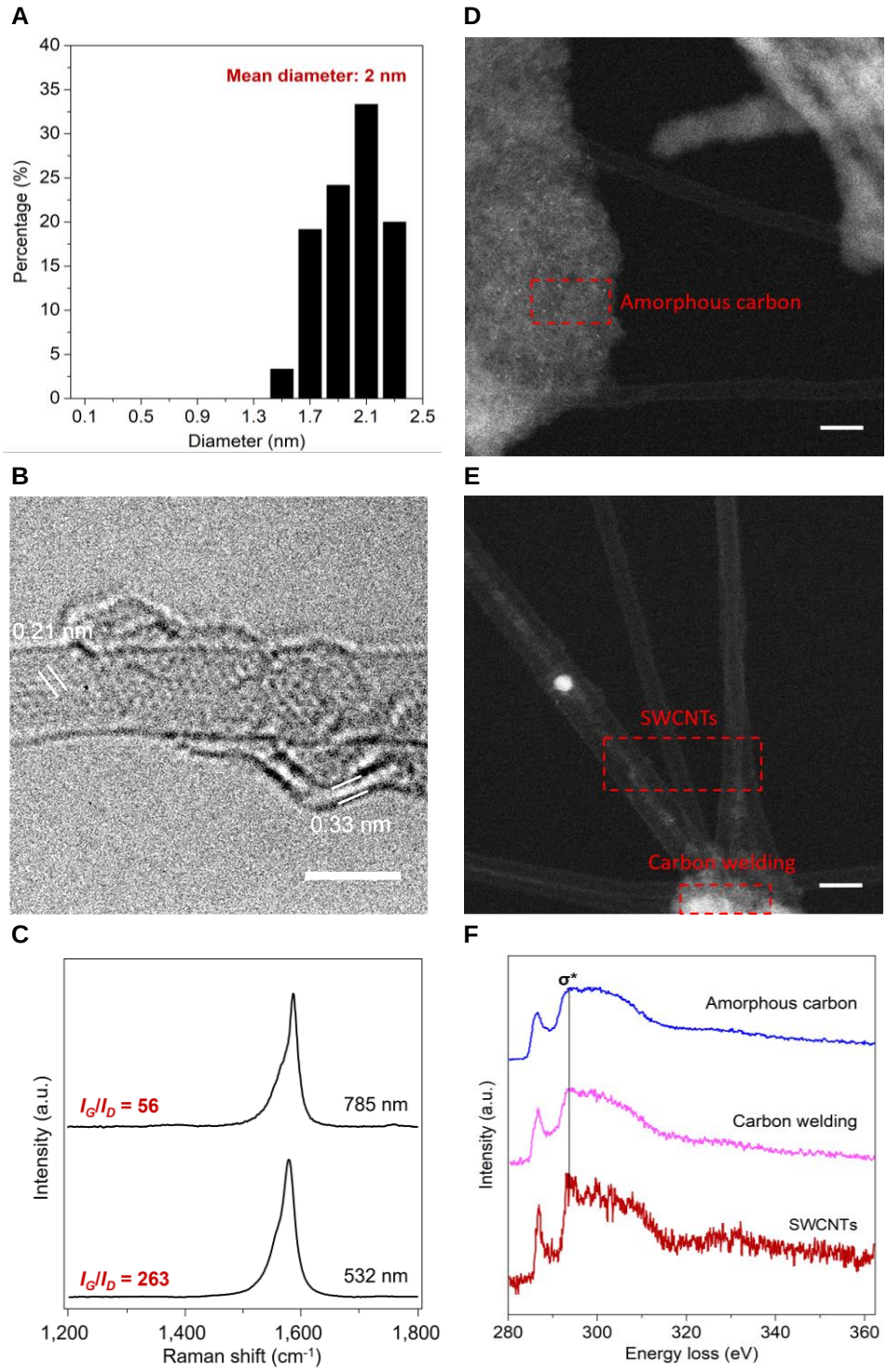

fig. S3. Microstructures of isolated SWCNTs with carbon-welded joints. (**A**) Diameter distribution of SWCNTs measured from TEM observations. (**B**) Typical high-resolution image of the surplus carbon. The scale bar is 2 nm. (**C**) Raman spectra excited by 532 and 785 nm lasers. (**D**) A STEM (Dark field) image of amorphous carbon on Cu grid. The scale bar is 5 nm. (**E**) A STEM (Dark field) image of SWCNTs

and carbon welding. The scale bar is 5 nm. (**F**) EELS spectra at C *K*-edge of the amorphous carbon, carbon welding and SWCNTs as marked with red rectangles in (C) and (D).

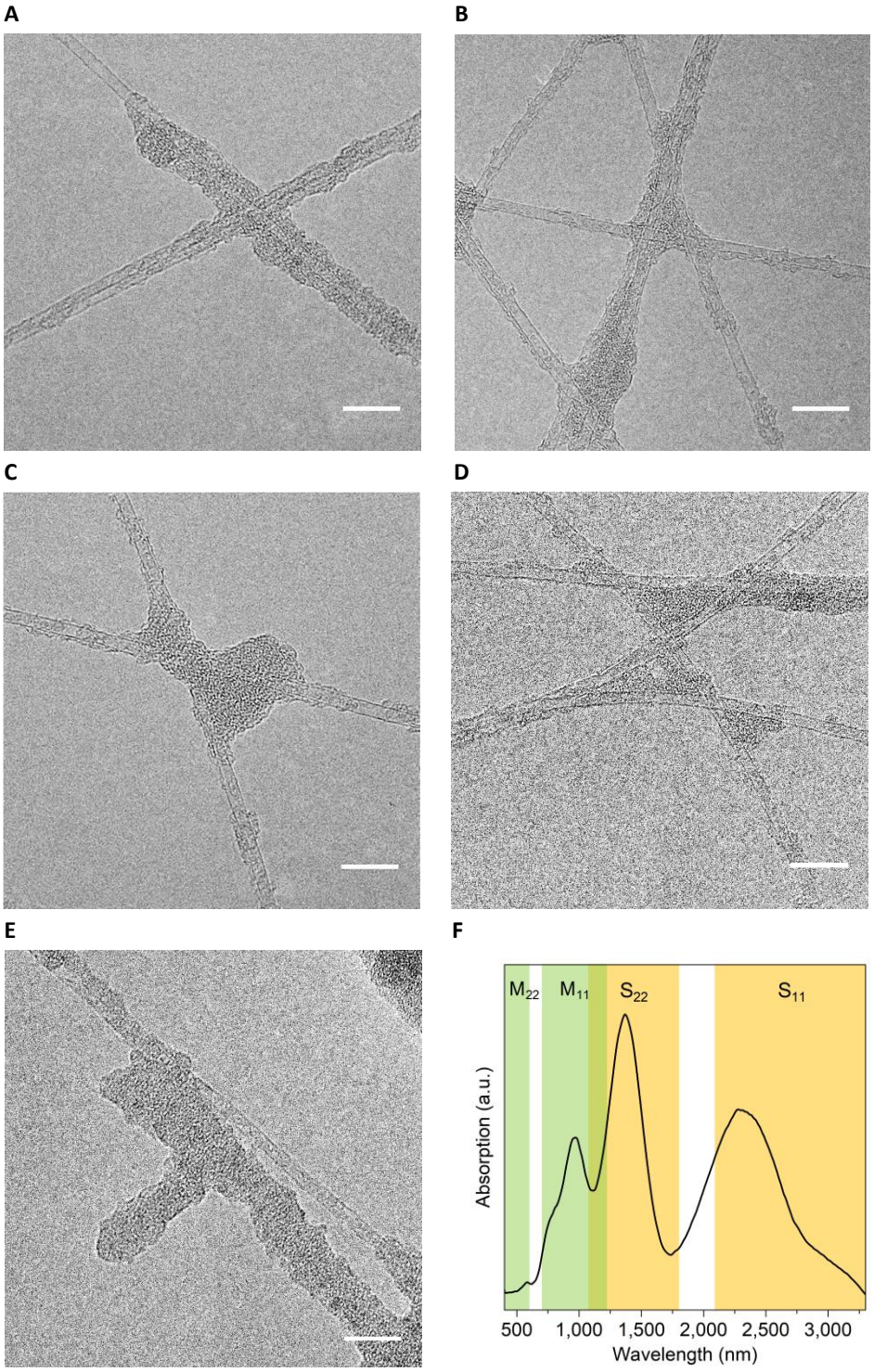

fig. S4. Thermal and optical characterizations. (**A**-**E**) Typical TEM images of the carbon-welded SWCNTs after heat treatment. (A) 400 ^{o}C, (B) 500 ^{o}C, (C) 600 ^{o}C, (D) 700 ^{o}C, (E) 750 ^{o}C. All the scale bars are 10 nm. In (A) to (D), no obvious change can be observed, demonstrating the high quality of the SWCNTs

and good stability of the carbon welding. (E) shows that most of SWCNTs have been destroyed, while the carbon welding material remains. (**F**) Absorption spectrum of the carbon-welded SWCNT film.

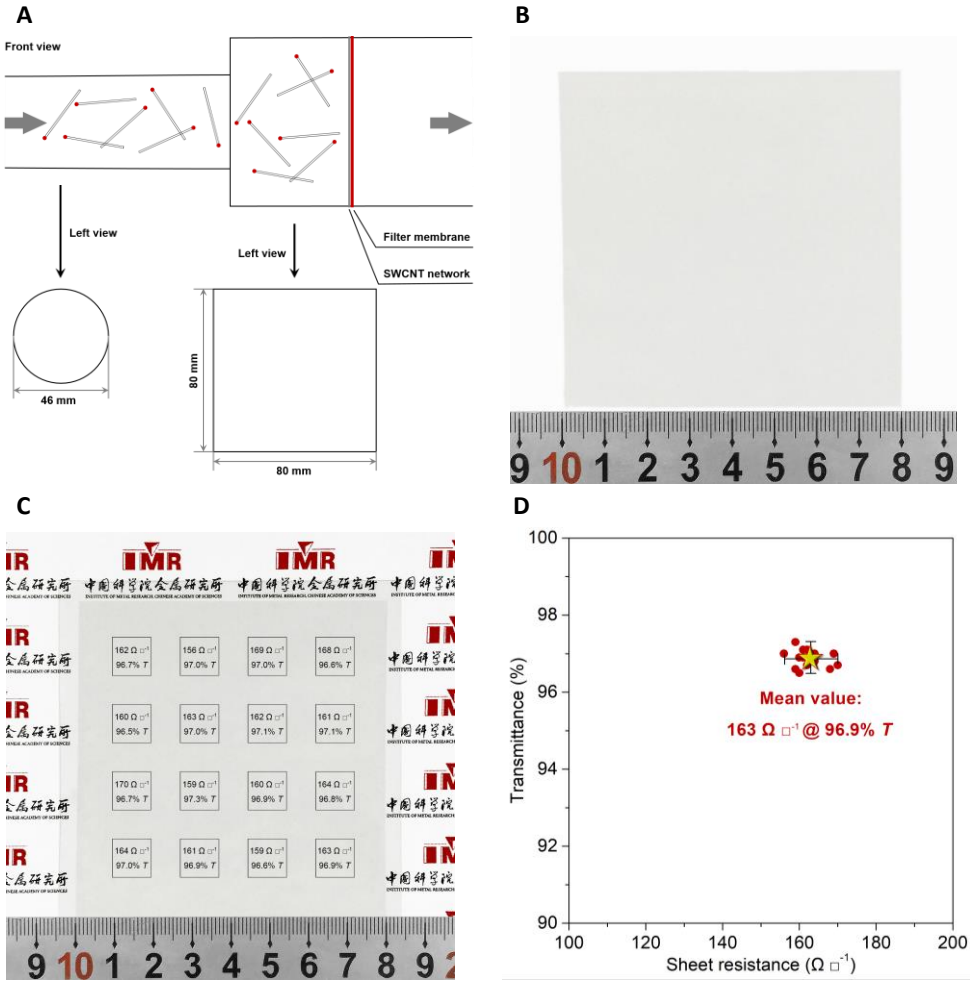

fig. S5. Experimental setup for preparing large-area SWCNT films and their characterizations. (**A**) Schematic of the collection process of large-area 80 mm × 80 mm SWCNT films. (**B**) Optical image of a collected SWCNT film deposited on a porous filter membrane. (**C**) Optical image of a transferred SWCNT TCF on a PET substrate with local R_S and T values labeled. (**D**) The statistics of T *versus* R_S at the 16 different locations in (C).

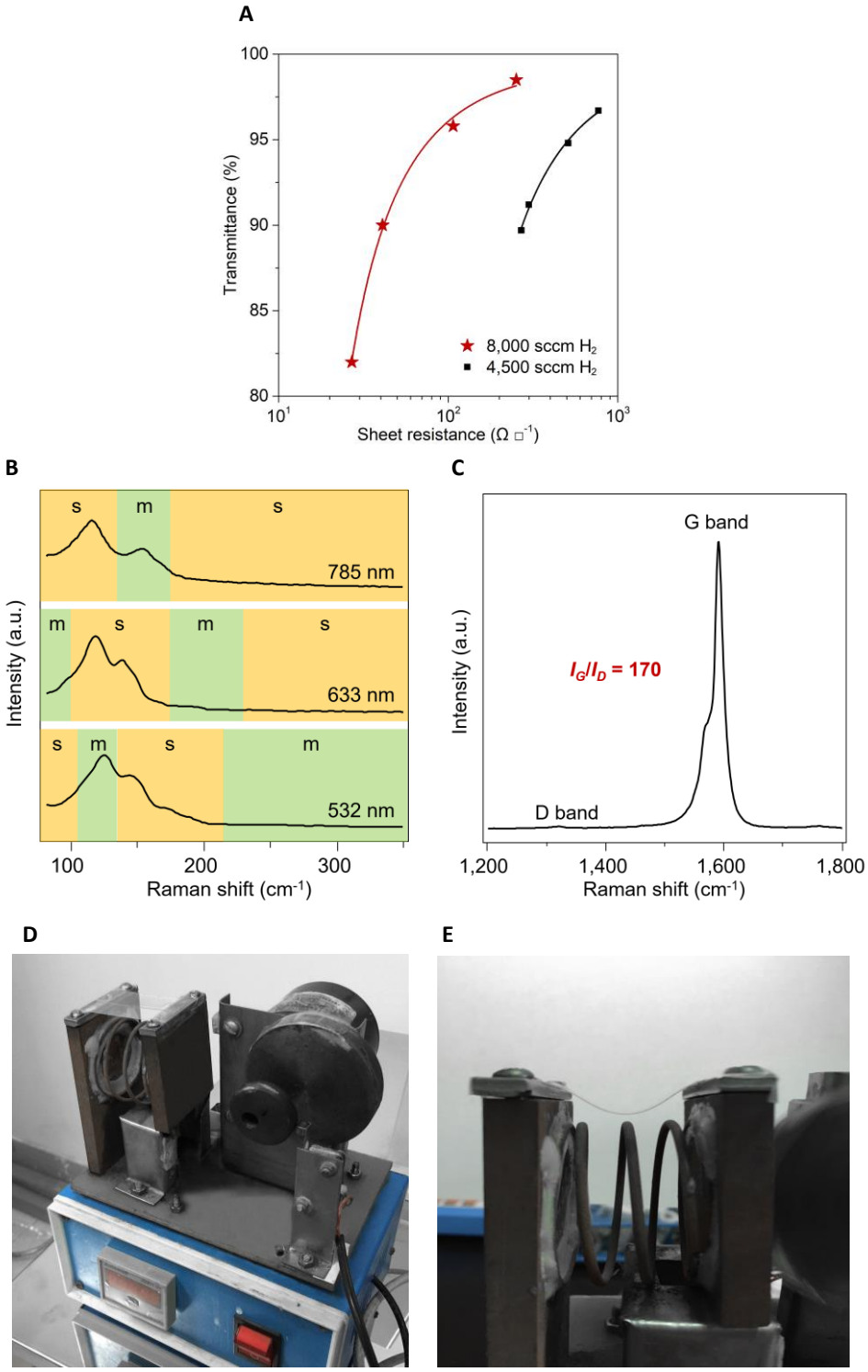

fig. S6. Optical, electrical, and mechanical characterizations of SWCNT films. (**A**)*T* (for 550 nm light) *versus* R_s of SWCNT TCFs synthesized using different-flux H_2**.** The typical performances of the SWCNT TCFs synthesized using 8,000 sccm and 4,500 sccm H_2 are 41 Ω □$^{-1}$ and 270 Ω □$^{-1}$ at 90% *T* for 550 nm light, respectively. (**B**) RBM mode Raman spectra of the normal bundled SWCNTs excited by 532, 633 and 785 nm lasers. (**C**) G and D bands of the Raman spectra of the normal bundled SWCNTs excited by

a 633 nm laser. (**D**) Oblique view of the bending test setup. (**E**) Front view of the bending test setup.

The TCFs were bent with an angle of 70° and a minimum radius of curvature of 5 mm.

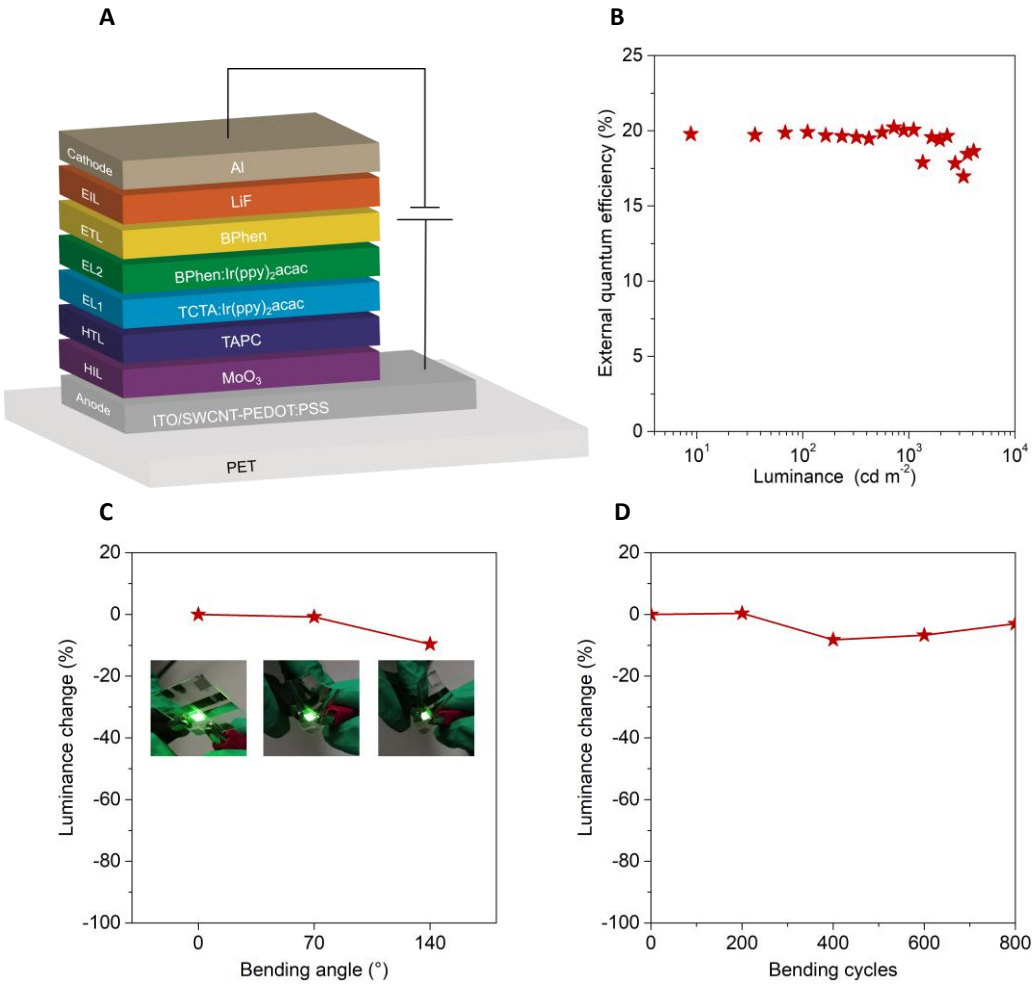

fig. S7. SWCNT OLEDs. (**A**) Schematic showing the structure of a SWCNT OLED. (**B**) External quantum efficiency *versus* luminance of the device. (**C**) Dependence of luminance change on bending angle of the flexible OLED with a minimum curvature radius of ~2 mm. (**D**) Dependence of luminance change of the OLED on bending cycles with a bending angle of 70° and a minimum curvature radius of ~4 mm.

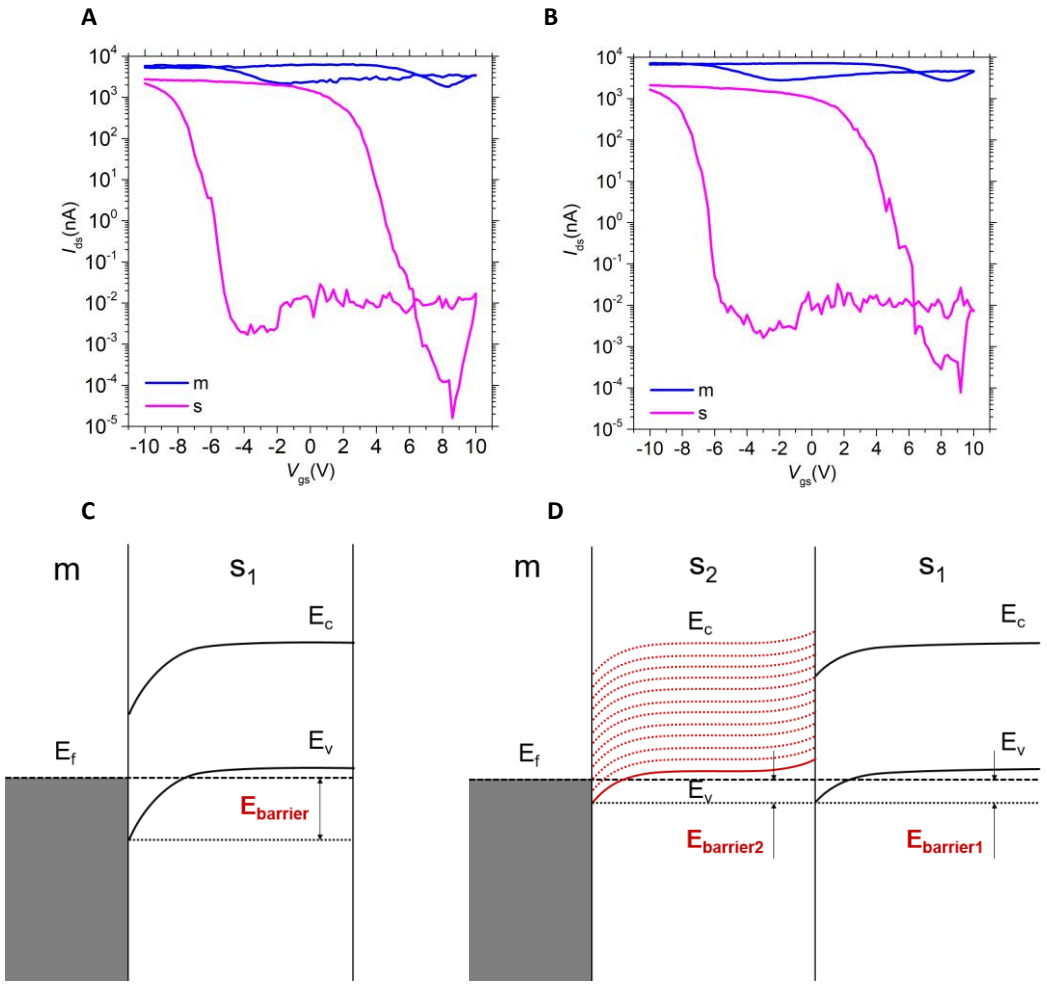

fig. S8. SWCNT FETs. (**A** and **B**) (A) and (B) show transfer characteristics I_{ds} *versus* V_{gs} curves of the SWCNTs shown in Fig. 5, A and C, respectively. V_{ds} = -1 V. The large hysteresis is mainly caused by charge traps originated from the adsorption of water molecules from ambient environment (*45*). (**C**) Schematic of the energy band at m-SWCNT (m)/s-SWCNT (s_1). (**D**) Schematic of the energy band at m-SWCNT (m)/carbon welding (s_2)/s-SWCNT (s_1). The red dotted lines indicate the bottoms of possible conduction bands of the carbon welding material formed from graphitic nanosheets with various sizes and edge structures.

table S1. Summary of the performance of pristine or doped SWCNT TCFs. (A) Summary of the performance of pristine SWCNT TCFs.

Fabrication method	Substrate	R_s ($\Omega\ \square^{-1}$)	T (550 nm light)	Year	Reference
Dry process	Quartz	950	90%	2016	(*4*)
Dry process	PET	~650	90%	2014	(*14*)
Dry process	Quartz	~635	95%	2015	(*15*)
		310	90%		
Dry process	Quartz	~410	95%	2014	(*18*)
		224	90%		
Dry process	Glass	50	70%	2007	(29)
Solution process	-	~231	75%	2008	(*30*)
Dry process	PET	252	98.5%	This work	
		107	95.8%		
		41	90%		
		27	82%		

(B) Summary of the performance of doped SWCNT TCFs.

Fabrication method	Substrate	Dopant	R_s ($\Omega\ \square^{-1}$)	T (550 nm light)	Year	Reference
Solution process	PET	CSA	60	90.9%	2011	(*2*)
Dry process	Quartz	HNO_3	63	90%	2015	(*3*)
Dry process	Quartz	HNO_3	89	90%	2016	(*4*)
Dry process + Patterning			29	87%		
Solution process	Quartz	HNO_3	30	70%	2004	(*12*)
Dry process	PET	HNO_3	160	90%	2014	(*14*)
Dry process	Quartz	$AuCl_3$	95	90%	2017	(*33*)
Dry process	PET	HNO_3	140	98.5%	This work	
			49	95.8%		
			25	90%		
			15	82%		

table S2. Chemical stability of a pristine SWCNT TCF evaluated by an accelerated aging test.

Sample	Before the accelerated aging test		After the accelerated aging test	
	T **(%)**	R_s **(Ω □$^{-1}$)**	***T*** **(%)**	R_s **(Ω □$^{-1}$)**
Pristine SWCNT TCF	90.0	41	89.8	38

Conditions of the accelerated aging test: 60 °C & 90% relative humidity for 250 h.